Novel Metastable Compounds in the Zr-B System: An *ab initio* Evolutionary Study

Jian Li, Changzeng Fan*

Abstract: Using *ab initio* evolutionary simulations, we explore the potential crystal structures with up to 18 atoms in the unit cell for all possible stoichiometries of the Zr-B system. In addition to the reported ZrB, ZrB_2, ZrB_{12}, oP8-ZrB and Zr_3B_4, two extraordinary Zr_2B_3 and Zr_3B_2 are found to be both mechanically and dynamically stable, as verified by the calculated elastic constants and phonon dispersions. The calculated formation enthalpies reveal that both new phases may be synthesized and found in experiments. It also reveals that the pressure is beneficial for the synthesis of all available phases except for the ZrB phase. In addition, the values of the Vicker's hardness for five Zr-B compounds are predicted by utilizing two different models. Contrary to the known hard phases of ZrB_2 and ZrB_{12}, the two new compounds are both having low values of hardness less than 10 GPa, consistent with their excellent ductility deduced from the bulk and shear moduli. Electronic structure calculations suggest that the new phases are both metallic, while electronic density maps show strong ionic bonding characteristics between Zr and B atoms. The crystal orbital Hamilton populations (COHP) diagrams have also been calculated in order to further analyze the bonding features of the

uncovered two novel phases.

Introduction

Transition-metal borides possess several unique properties among which are high melting points, hardness, inertia, chemical stability, and metallic property as seen in transition-metal carbides.[1-3] Combination of these properties in some systems make them to be of considerable technological importance and therefore have become the subject of several experimental and theoretical studies in the past decades.[4-5] Among these transition-metal borides, Zirconium-boron (Zr-B) system is a rather typical one and has attracted substantial interest owning to its extreme chemical and physical properties.[6-11]

To the best of our knowledge, there are three phases, namely ZrB, ZrB_2, and ZrB_{12} have been reported and widely studied for this system:

(1) ZrB phase. According to the Zr-B phase diagram,[10, 12-14] zirconium monoboride (ZrB) can exist in the range from 1073 to 1523 K.[15] Although Rudy and Windisch [16] along with Portnoi and Romashov[17, 18] failed to observe this phase in their experimental study, its existence was confirmed later by Nowotny *et al*..[19] Champion and Hagege [8, 9, 20] further confirmed the existence of ZrB with peritectoid reaction by XRD and TEM analysis, and even found that this phase was easily stabilized to room temperature. Moreover, this phase was identified with the NaCl type structure (space group $Fm\bar{3}m$, No. 225) by selected-area electron and

X-ray diffraction, and the lattice parameter of which, measured by X-ray experiments, is about 4.71 Å.[9]

(2) ZrB_2 phase. From the B-Zr phase diagram, one can find that ZrB_2 is the most stable compound.[12-14] As a sound member of ultra-high temperature ceramics (UHTCs) family, this phase has gained much attention in the past few years. In addition to sufficiently high melting point and hardness, ZrB_2 has a great deal of unique properties including high thermal and electrical conductivity, low work function, as well as oxidation resistance.[21, 22] These unique and intriguing characteristics have inspired the scientists to develop them as thermal protection materials for future hypersonic aerospace vehicles and other high-temperature structural applications.[23-26] The crystal structure of ZrB_2 is hexagonal (AlB_2 type，space group *P6/mmm*, No. 191) with cell parameters of a=3.169 and c=3.530 Å.[27] Except for the simple crystal structural data, the diverse properties of ZrB_2 have been investigated experimentally and theorectically.[28-30]

(3) ZrB_{12} phase. According to the work of Glaser and Post, [15] ZrB_{12} is unstable below 1873 K. A full range of stability between 1073 and 2303 K was shown by Portnoi and Romashov.[17] Further, Rudy and Windisch[16] proved that the eutectoid decomposition of ZrB_{12} on cooling into ZrB_2 and hcp-Zr at 1983±15 K by DTA-experiments. Later, Rogl and Potter[7] confirmed the instability of this phase below 1973 K. The crystal

structure of this compound is characterized by a three-dimensional boron network, and it can be described as B_{12} cubo-octahedral units located at the corners and face centers of a cube, namely UB_{12}-type structure (space group $Fm\overline{3}m$, No. 225).[31] Detailed structural information can be found in Table S1 of the supplementary file. Moreover, ZrB_{12} is one such compound exhibiting relatively high superconducting transition temperature of 6 K in the MB_{12} family.[32] Beyond that, many other properties also attracted considerable interest in this compound.[33-36]

Apart from the above mentioned three phases, a comprehensive investigation conducted by Callmer *et al*.[37] showed a maximum solubility of 2 at.% in β-B corresponding to the composition ZrB_{51} at 2023 K by quantitatively full profile Rietveld refinement of X-ray powder diffraction of the arc melted sample. Based on estimated heat of formation data of the compounds, Rogl and Potter[7] speculated the metastablity of Zr_3B_4 and another ZrB phases (space group oP8, hereafter denoted as *oP8*-ZrB).

In the present work, we explore the possible stable stoichiometries in the Zr-B system and indeed find two new stoichiometries (Zr_2B_3 and Zr_3B_2) to be stable by using *ab initio* evolutionary algorithm USPEX.[38-40] The stability of these new phases is determined by elastic constants and phonon spectra. Further calculations are performed to study the mechanical and electronic properties of the two new phases.

Calculation Methods

Evolutionary algorithms are well-suited for the task of crystal structure prediction: using "learning" from the history of the simulation, evolution guides search towards low-energy structures; improving the results from generation to generation, such simulations "zoom" in on the most promising part of the energy landscape until the lowest-energy structure is found. All evolutionary simulations were performed with the USPEX code, using VASP for structure relaxation and energy calculation.[41] Any combinations of numbers of atoms in the unit cell were allowed (with the total numbers ≤ 18) and calculations were performed at pressures of 0 ~ 30 GPa. The first generation of structures was created randomly and the number of structures in the population was set to 200. The upper 60% of each generation were used to produce the next-generation structures by heredity. The rest are produced by soft mutation (20%), random space group specificity (10%), and lattice mutation (10%). The best structure of previous generation was set to survive and compete in the following generation. Forty generations (maximum) was required in our global optimisation.

Once a new structure was obtained from USPEX, the structural relaxation and properties calculations were implemented in the VASP code, which were carried out using the all-electron projector-augmented wave (PAW) method[42] within the framework of density functional theory.[43] The exchange correlation potentials were treated within the generalized gradient approximation (GGA) of Perdew-Burke-Ernzerhof (PBE).[44] Convergence of different xc-functionals of DFT has been tested and provided as supplementary information. The PAW pseudopotentials[45] are adopted, with $4s^2p^6d^25s^2$ and $2s^2p^1$ electrons were considered as the valence electrons for Zr and B atoms, respectively. The cutoff energy (420 eV) for the expansion of the wave function into plane waves was chosen to ensure that the results are in accordance with the convergence criteria. The *k*-points samplings in the Brillouin zone are 6×11×5 for the Zr_2B_3 phase and 3×11×10 for the Zr_3B_2 phase based on the Monkhorst-Pack method.[46] More k-points such as 2000 and 4000 in total in the whole Brillouin zone have also been tested and no contradicting results have been found.

To ensure that the obtained structures are dynamically stable, we calculated phonon frequencies throughout the Brillouin zone using the finite-displacement implemented in the Phonopy code.[47] The calculation of the elastic constant was carried out using the CASTEP code.[48]

To elucidate the bonding information in these new phases, we adopted a variant of the familiar COHP approach that stems from a PW calculation and was dubbed “projected COHP” (pCOHP).[49, 50] In this approach, all the projection and analytic methods have been implemented in a standalone computer program —LOBSTER— is built to read and process output data from plane-wave DFT packages (here is VASP code).

By re-extracting atom-resolved information from the delocalized plane-wave basis sets, that is processing the PAW parameters and self-consistent results from VASP, LOBSTER can give us access to projected COHP curves, which we can use to visualize the chemical-bonding information in our DFT calculations.

Results and discussion

Optimized crystal structures

The schematic ambient crystal structure of Zr_2B_3 is projected along the [100] and [010] directions, respectively, as shown in Figure 1 (a) and (b). This phase belongs to orthorhombic crystal system (space group *Pmmn*, No. 59), and the unit cell is composed of 10 atoms. Both Zr and B have two non-equivalent sites in this structure, of which Zr1 and B1 atoms occupy Wyckoff 2*a* and 4*f* positions, while the other Zr and B atoms (Zr2 and B2) take the 2*b* position. For this phase, the coordination environments are complex (for the convenience of description, we take two atoms separated as long as 2.672 Å still forming a “bond”): every Zr1 atom is bonded with the surrounding six B1 and four B2 atoms, and four types of Zr-B bonds with bond lengths of 2.499, 2.524, 2.619 and 2.672 Å are found; while the Zr2 atom is bonded to six B1 atoms and one B2 atom, and three types of Zr-B bonds with bond lengths of 2.372, 2.534 and 2.612 Å exist – see Figure 1 (c). Considering the B atoms, the coordination environments are also quite different: each B1 is bonded to three Zr1, three Zr2, one B1 and two B2 atoms, forming two types of B-B bonds (1.737 and 1.894 Å) and four types of Zr-B bonds with bond lengths of 2.524, 2.534, 2.612 and 2.672 Å; while each B2 atom is bonded to four Zr1, one Zr2 and four B1 atoms, forming only one type of B-B bond (1.894 Å) and three types of Zr-B bonds with bond lengths of 2.372, 2.499 and 2.619 Å, as plotted in Figure 1(d). In summary, there are seven types of Zr-B bonds with distances ranging from 2.372 to 2.672 Å and two types of B-B bonds with bond lengths of 1.737 and 1.894 Å. The detailed optimized crystallographic data of this phase is listed in Table 1.

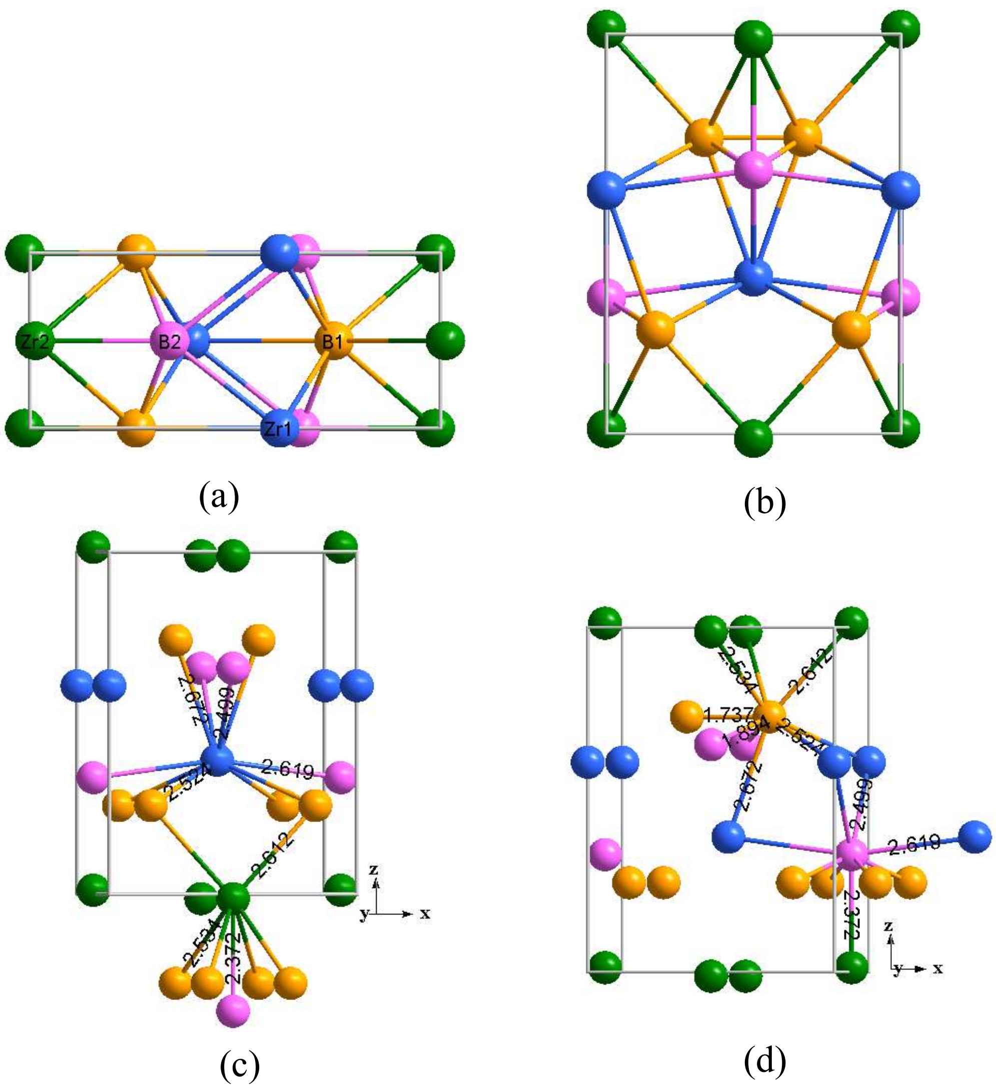

(a) (b)

(c) (d)

Fig. 1 Schematic image of Zr_2B_3 is projected along the [100] and [010] directions, respectively [(a) and (b)]; (c) the coordination environment of Zr1 and Zr2 atoms; (d) the coordination environment of B1 and B2 atoms. Zr1, Zr2, B1 and B2 atoms are denoted in blue, green, orange and pink, respectively.

The schematic ambient crystal structure of Zr_3B_2 is shown in Figure 2(a), suggesting an orthorhombic structure with the space group *Cmmm*. There are 10 atoms in the unit cell, of which B and two non-equivalent Zr (Zr1 and Zr2) atoms occupy Wyckoff 4*g*, 2*a* and 4*h* positions, respectively. Structurally, if we consider the area in the dashed box as an entity, there is another symmetric entity on the other side of the red dotted line (see Figure 2(a)).Then the new structure of Zr-B forms by place them into high symmetry positions of a cuboid lattice with Zr1 atoms. An entity is composed of several Zr2 and B atoms, which is projected along the [100] and [001] directions, respectively, as shown in Figure 2(b) and (c). The Zr2 atoms are coordinated by six B atoms, whereas the B atoms are coordinated by six Zr2 atoms and two B atoms. In total, there are one type of Zr-B bond and two types of B-B bonds, as illustrated in Figure 2 (b) and (c) along with their bond lengths. The detailed optimized crystallographic data of this phase can be found in Table 2.

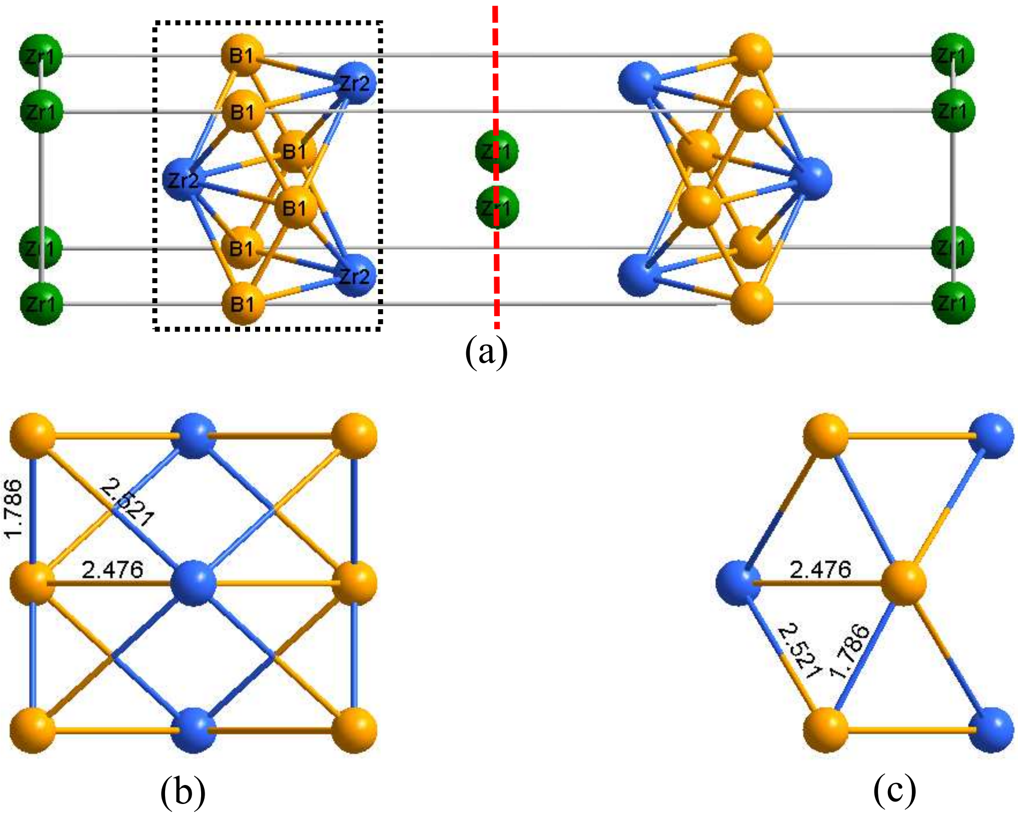

Fig. 2 Schematic image of (a) Zr_3B_2; the area in the dashed box [Figure (a)] projected along the [100] and [001] directions, respectively [(b) and (c)]. Zr1, Zr2 and B1 atoms are denoted in green, blue and orange, respectively.

Stabilities of new phases

To verify the mechanical stability of the new phases of Zr-B system, the elastic stiffness constants of the phases that kept their structures at the ground state after full optimizations were calculated and summarized in Table 3. Because both of these two new phases belong to the orthorhombic crystal system, thus there are nine independent elastic constants. For the orthorhombic crystal, the corresponding mechanical stability criterion[51] is as follows:

$$C_{ii} > 0\ (i = 1, 2, 3, 4, 5, 6) \qquad C_{11} + C_{22} + C_{33} + 2(C_{12} + C_{13} + C_{23}) > 0$$

$$C_{11} + C_{22} - 2C_{12} > 0 \qquad C_{11} + C_{33} - 2C_{13} > 0 \qquad C_{22} + C_{33} - 2C_{23} > 0 \qquad (1)$$

According to the criterion and values in Table 3, the phases considered are both mechanically stable at the ground state.

Dynamically stability is also important for a structure, as the appearance of soft phonon modes will lead to the distortion of the crystal. Phonon dispersions in the whole Brillouin zone of the Zr_2B_3 and Zr_3B_2 are plotted in Figure 3. The inexistence of imaginary frequencies indicates the dynamic stability of the new phases. Therefore, being both mechanically and dynamically stable, the new phases may find some technological applications in future.

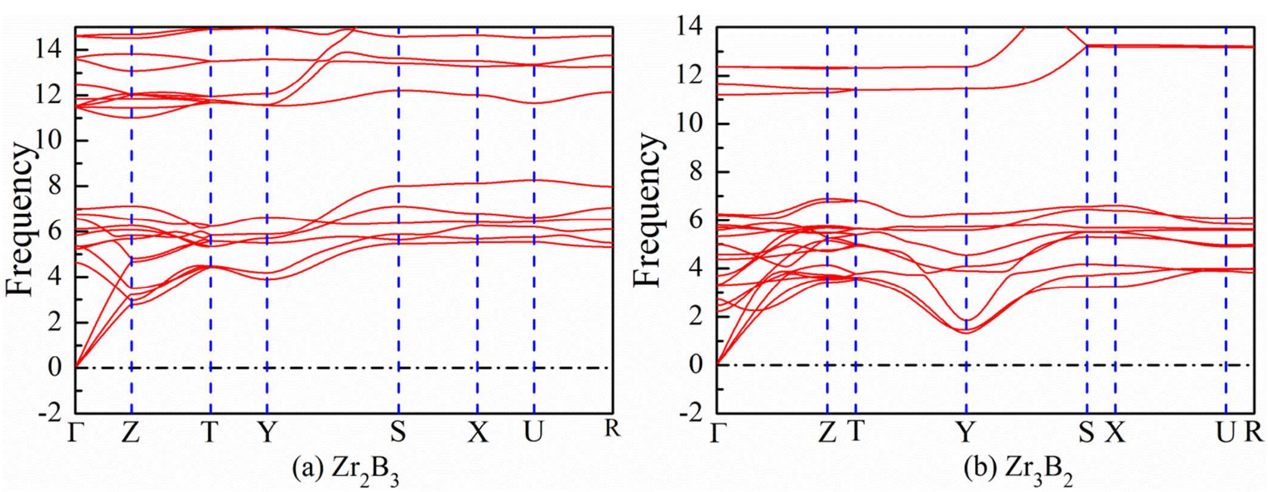

Fig. 3 Phonon dispersion curves for the newly discovered Zr-B phases.

To further validate the thermodynamic stability of the studied compounds, we also calculated the convex hull, which is defined as a formation enthalpy versus composition diagram with "breaking points" (*i.e.*, the ground state) at special compositions. Figure 4 shows that among the considered phases at 0 ~ 50 GPa, our calculations yield a ground state convex hull defined by two structures: ZrB_{12} and ZrB_2, which were observed experimentally. Most remarkably, the minimum of formation enthalpy is reached at that of ZrB_2. The formation enthalpies of Zr_2B_3, Zr_3B_2, ZrB, oP8-ZrB and Zr_3B_4 lie above the solid line of convex hull, indicating they are thermodynamically unstable relative to ZrB_2 and Zr. However, at zero pressure, Zr_3B_2 lies above the line connecting the values for ZrB_2+Zr by about 71.4 meV/atom, which is comparable to those of oP8-ZrB and Zr_3B_4 (73.3 and 47.7 meV/atom above the line respectively, which are in reasonable agreement with Ref.11). Rogl and Potter[7] estimated that oP8-ZrB and Zr_3B_4 may be stable below 529℃, thus Zr_3B_2 might also be synthesized at high pressure and/or high temperature. In addition, Zr_2B_3 may be synthesized according to the reaction: $ZrB_2 + ZrB \rightarrow Zr_2B_3$. Furthermore, their enthalpies of formation are greatly enhanced by increasing pressure except for the ZrB phase, indicating that pressure is beneficial for the synthesis of these phases. ZrB has largest distance (about 369.2 meV/atom) from the convex hull in the studied pressure interval, which may explain why it is seldom synthesized and found in experiments. However, we would like to emphasize that, if one carefully control the stoichiometry and experimental conditions, the uncovered two phases of Zr_3B_2 and Zr_2B_3 may be synthesized, either at ambient pressure or elevated pressure/temperature. For the ZrB phase, the effect of pressure on its enthalpy of formation is not very significant. When the pressure increases, the enthalpy decreases firstly, and then increases again, as shown in the inset of Figure 4.

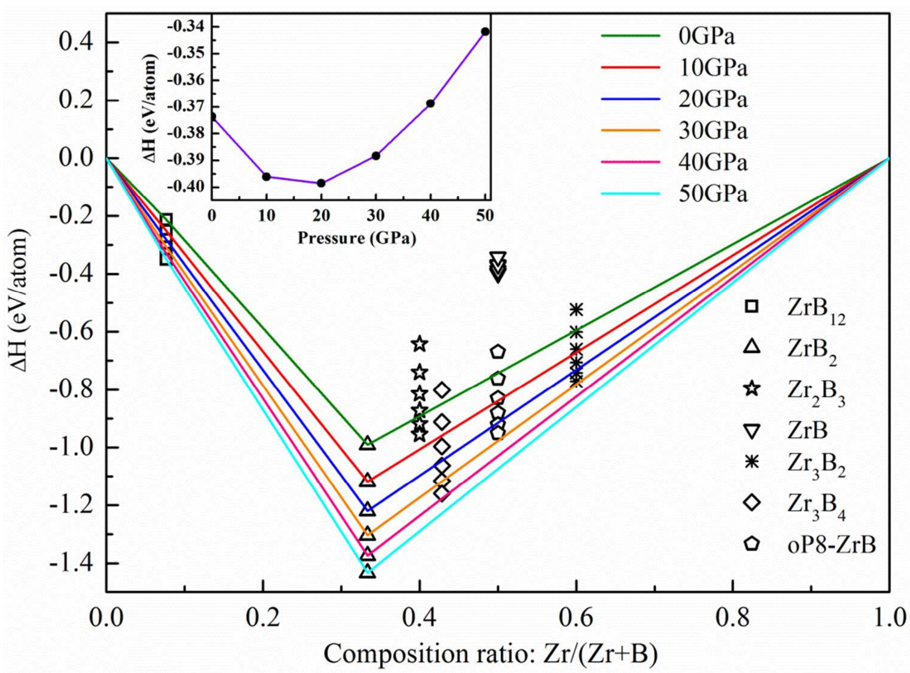

Fig. 4 The convex hull of Zr-B system at the pressure of 0 ~ 50 GPa. The solid line indicates the convex hull. The enthalpy of formation of ZrB as a function of pressure is also shown in the inset.

Mechanical properties

The mechanical properties of the new two structures are investigated for their potential applications. On the basis of the Voigt-Reuss-Hill approximation, [52] the corresponding bulk and shear modulus (B and G) are obtained from the calculated elastic constants at ambient pressure. The Young′s modulus (E) and the Poisson′s ratio (σ) are then calculated by using the following relations:

$$E = \frac{9BG}{3B+G} \quad , \qquad \sigma = \frac{3B-2G}{2(3B+G)} \tag{2}$$

The values of B, G, E, σ and B/G are illustrated in Table 4.

As shown in Table 4, the bulk modulus, shear modulus, Young′s modulus values of the new Zr_2B_3 and Zr_3B_2 phases are much lower than those of the known phases, suggesting the new discovered phases of Zr-B are more compressible than the known ones.

According to the Pugh′s criterion, [54] the ratio value of B/G is commonly used to describe the ductility or brittleness of materials with 1.75 as the critical value. A material can be described as brittle (ductile) if the B/G ratio is less (more) than 1.75. Interestingly, the B/G values of all known Zr-B phases are less than 1.75 while those of the new two phases are both exceed 1.75. Therefore, contrary to the known compounds of Zr-B in a brittle manner, the new predicted compounds would behave in a ductile manner.

The vicker′s hardness of both new phases are firstly calculated by adopting the empirical scheme[55] which correlates the Vicker′s hardness and the Pugh′s modulus ratio through the formula

$$H_v = 2(\kappa^2 G)^{0.585} - 3, \qquad \kappa = G/B \tag{3}$$

According to Eq. (3), the obtained values of Vicker′s hardness (H_v^*) are illustrated in Table 4. To give a range of possible values, we also use the Lyakhov-Oganov method[56] to evaluate the Vicker′s hardness values ($H_v^\#$)

of both structures – also see Table 4. To use the formula of hardness given by Lyakhov and Oganov, we need to use the structure file POSCAR (which must contain an element symbol line) aandd set the parameters for goodBonds, valence and valence electrons. For main group elements, only the outermost electrons are considered as valence electrons under normal circumstances. The hardness values H_v^* and $H_v^\#$ of the known phases ZrB, ZrB_2 and ZrB_{12} are calculated with the literature data and experimental structures, respectively. From the data, the results from the two models agree very well. Not surprisingly, the values of hardness of the newly discovered phases are both less than 10 GPa, which is not comparable to those of the known phases. However, such soft feature along with the good ductile character may cause them to be of considerable special technological application.

Figure 5 (a) and (b) plot the pressure dependence of the lattice constants *a*, *b*, and *c* for Zr_2B_3 and Zr_3B_2 up to 50 GPa. It can be seen that the *b* axis is the most incompressible crystallographic direction for both structures. One can notice that for the case of Zr_2B_3, *a* and *c* axes exhibit similar compressibility at relatively lower pressure, the *c* axis becomes much easier compressed than that of *a* axis as the pressure further increases. Concerning the phase Zr_3B_2, the *a* axis is much easier compressed than both *b* and *c* axis in the whole studied pressure range. The pressure dependence of cell volume is also shown in the insets.

Comparatively, the rate of the volume shrinkage for Zr_3B_2 (about 21.6%) is larger than that of Zr_2B_3 (16.7%), resulting in a remarkably smaller bulk modulus than that of Zr_2B_3 (see Table 4).

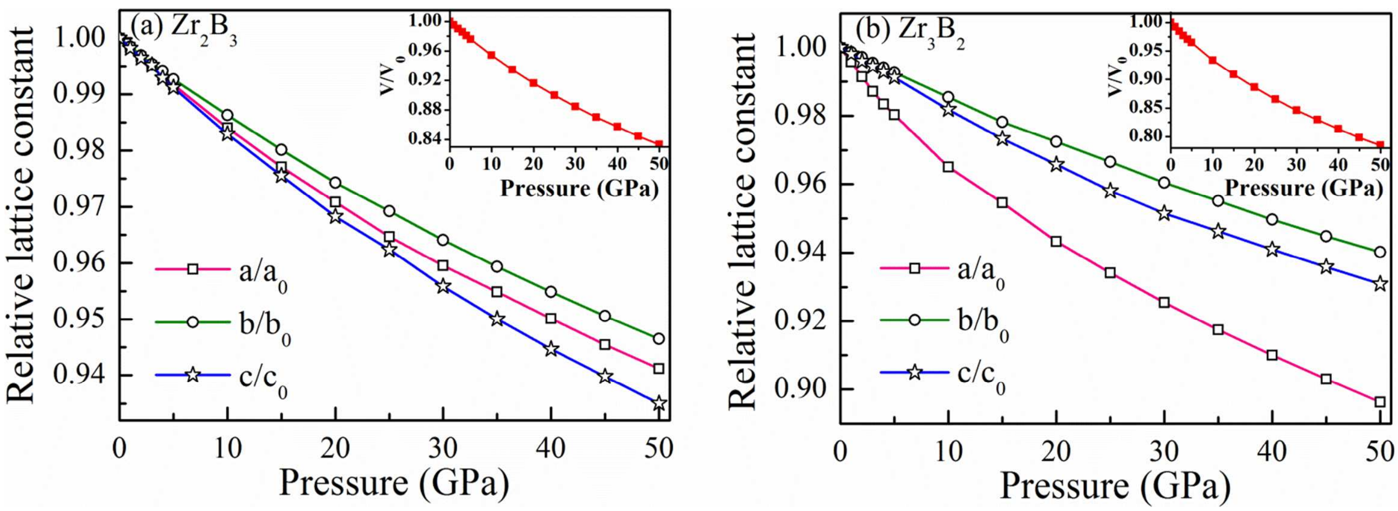

Fig. 5 Pressure dependence of lattice constants *a*, *b* and *c* for (a) Zr_2B_3 and (b) Zr_3B_2. The pressure dependence of cell volume is also shown in the inset.

Electronic structure and chemical bonding

The electronic properties of both phases were investigated by analyzing their electronic band structure and partial density of states (PDOS). It can be clearly seen that the two new phases are metallic as the energy bands crossing over the Fermi level (E_f), which is quite similar to the known Zr-B phases, as shown in Figure 6.

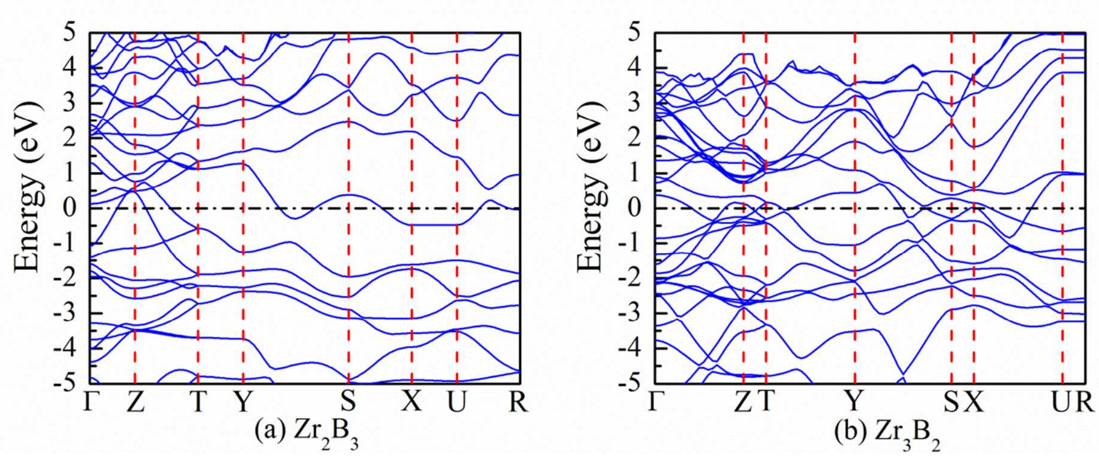

Fig. 6 Calculated band structure for Zr_2B_3 and Zr_3B_2 at ambient pressure.

The calculated PDOS for Zr_2B_3 is shown in Figure 7 (a). It is clear from the figure that the valence band can be separated into two regions (-2.5 eV as the dividing point). The low energy region is dominated by B 2*p* state, and the Zr 4*d* orbital and B 2*p* orbital show some extent of hybridization, while the upper energy region originates mainly from the contribution of Zr 4*d* orbital. The 4*d* state extends into and above the Fermi energy level and shows a weak hybridization with the B 2*p* state. For the Zr_3B_2 phase, the situation is similar to that of Zr_2B_3 except for the very weak hybridization between B 2*p* and Zr 4*d* states in the low part of valence band (-2.6 eV as the dividing point) – see Figure 7 (b). Meanwhile, near the Fermi level, the Zr 4*d* orbital dominates the conduction properties, whereas the B atoms contribute little. The total electronic DOS of the Fermi level for the Zr_2B_3 phase is 4.2 states per eV, which is smaller than that of the Zr_3B_2 phase (6.1 states per eV), indicating that the Zr_3B_2 phase may have more conducting electrons at Fermi level than that of Zr_2B_3.

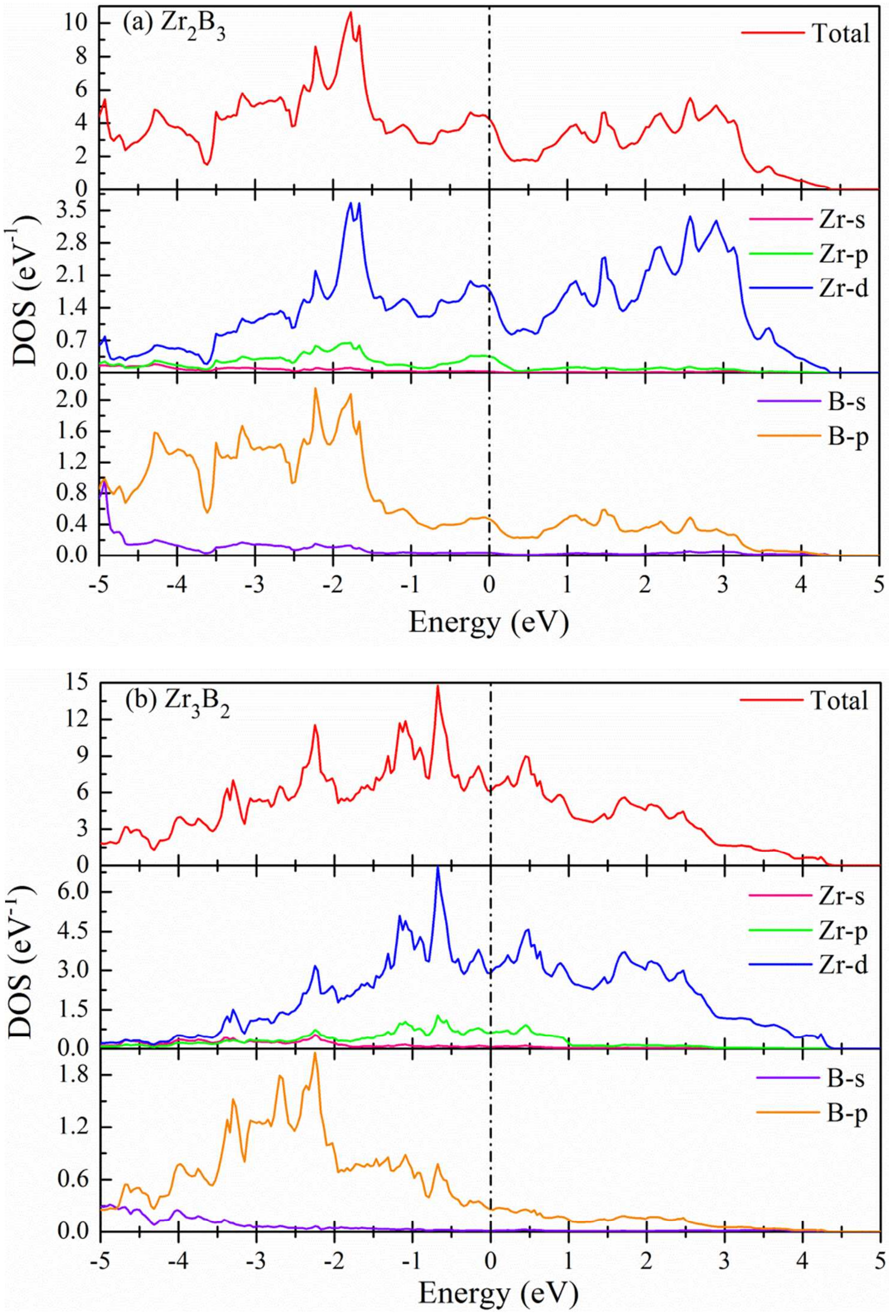

Fig. 7 Partial densities of states for (a) Zr_2B_3 and (b) Zr_3B_2.

Figure 8 exhibits the calculated charge density distribution of Zr_2B_3 and Zr_3B_2 along the (010) plane. Charge density distributions server as a complementary tool and can provide a proper understanding of the electronic structure and bonding features of the system. From Fig. 8 (a) and (b), there are some electrons gather around the Zr atoms, whereas no electrons distribution around the B atoms, which suggest significant charge transfer from B to Zr atoms and a ionic feature of bonding between Zr and B atoms in both the Zr_2B_3 and Zr_3B_2 phases.

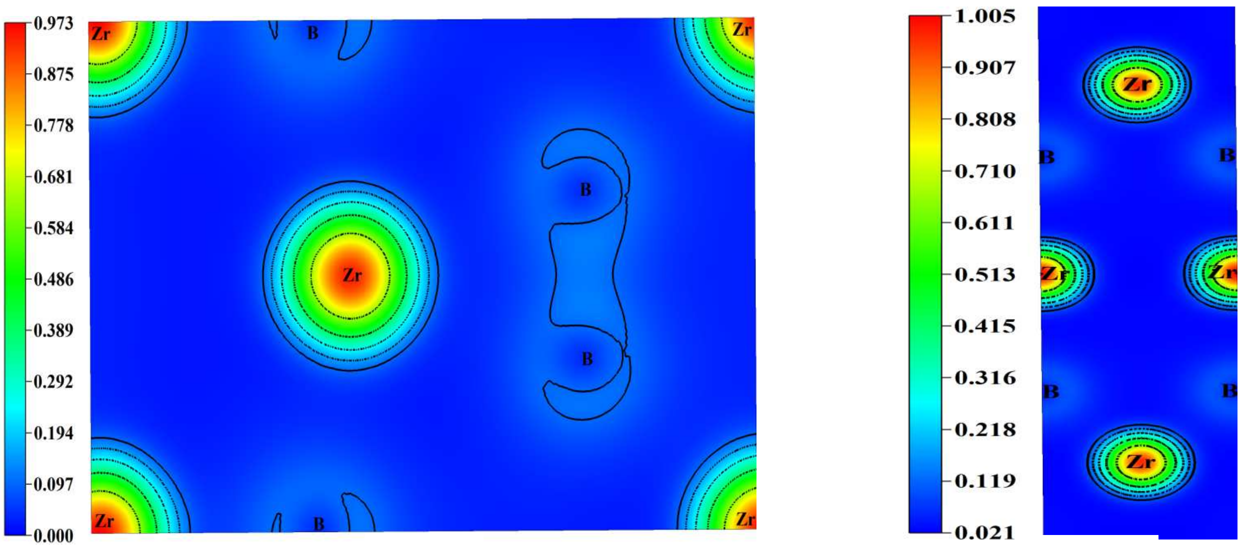

(a) (b)

Fig. 8 The charge-density distribution maps for the selected slices of (a) Zr_2B_3 and (b) Zr_3B_2.

Another technique named the crystal orbital overlap population (COOP) [57, 58] and its analogous crystal orbital Hamilton population (COHP) [59, 60] which is a bond-detecting tool for solids and molecules, can provide a straightforward view onto orbital-pair interactions. The COHP analysis was introduced in 1993, which is a partitioning of the band structure energy in terms of orbital-pair contributions. Therefore it is based on a local basis as is commonly used in chemistry and parts of physics as well. Based on these techniques, one can analyse and interpret the bonding situation in solid-state materials. To elucidate the bonding situation in the new phases, the COHP analysis was performed in the present work. COHP partitions the band structure energy (in term of the orbital pair contributions) into bonding, nonbonding and antibonding energy regions within a specified energy range. We plot –pCOHP (projected COHP) and IpCOHP (integrated pCOHP) as a function of energy for the Zr-B and B-B interactions in the structures of Zr_2B_3 and Zr_3B_2, as shown in Figure 9 (a) and (b), respectively. Positive values of –pCOHP describe bonding energy regions whereas negative values describe antibonding energy regions. As seen from the COHP diagram in Fig. 9(a), the composition Zr_2B_3 is characterized by massively bonding Zr-B interactions near the Fermi level, however, for B-B bonds there exist obvious antibonding states. Concerning the Zr_3B_2 phase, as is evident from Fig. 9(b), we find an opposite phenomenon where Zr-B bonds exhibit a certain density of antibonding states at Fermi level while B-B bonds show bonding states at Fermi level.. For the B-B bonds of the two new phases, whose bonding energy (IpCOHP) is higher than that of the Zr-B bonds, suggesting the interaction between the anions and the anions in both phases is stronger than that of cation-anion bonding.

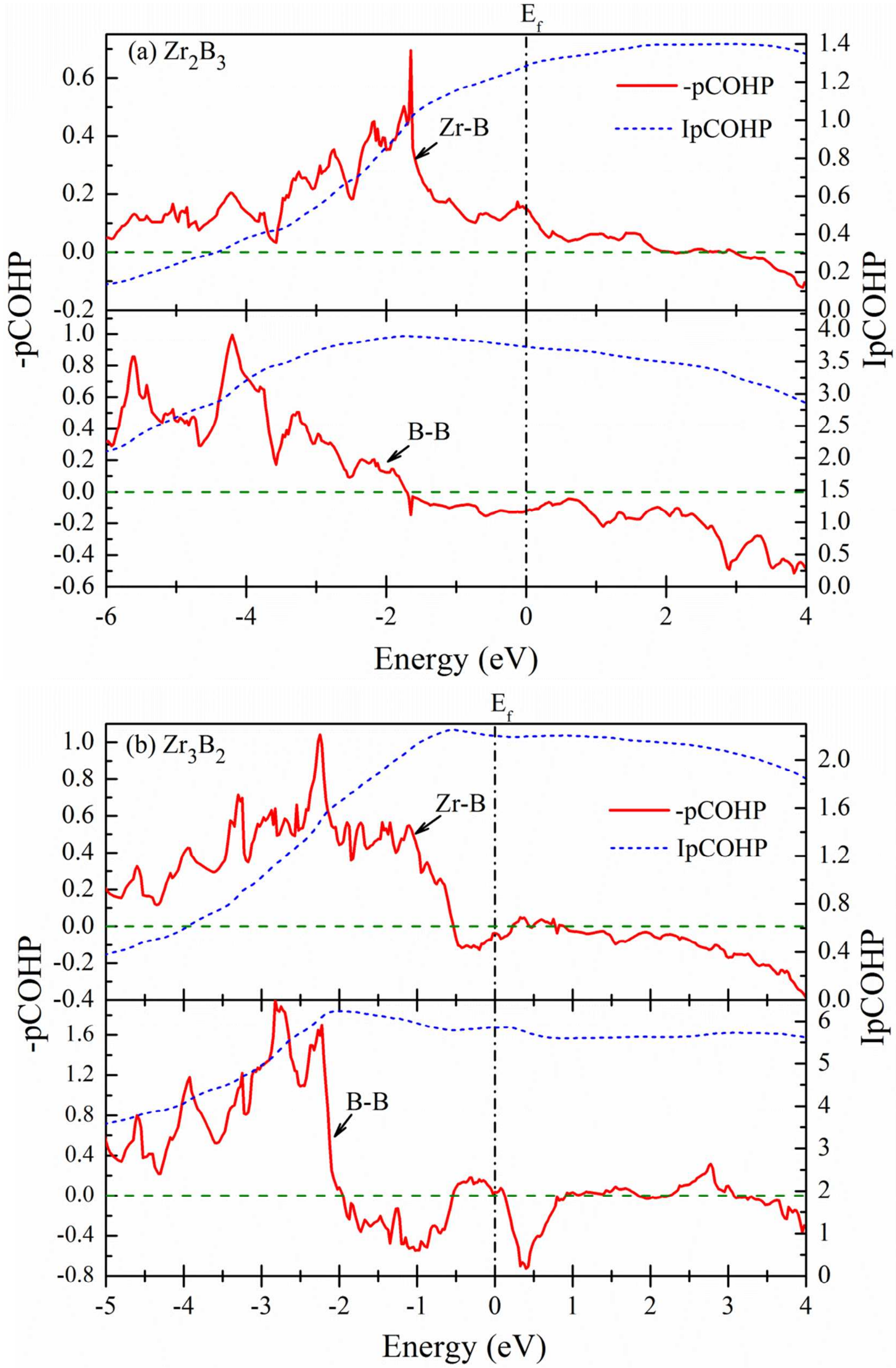

Fig. 9 Crystal orbital Hamilton population (pCOHP) analyses for the new phases are obtained with the PW/PAW-based method.

Conclusions

In summary, we performed a systematic search for possible stoichiometries in the Zr-B system. Except the well-known compounds, two more stoichiometries (Zr_2B_3 and Zr_3B_2) have been found. Phonon dispersions and elastic constants calculations suggest the stability of the new phase. The formation enthalpy of Zr_3B_2 phase is comparable to those of oP8-ZrB and Zr_3B_4, implying it may be synthesized and found in experiments. In addition, Zr_2B_3 may be synthesized according to the reaction: $ZrB_2 + ZrB \rightarrow Zr_2B_3$. Moreover, it is found that the pressure is beneficial for the synthesis all these phases except for the ZrB phase. The values of the predicted hardness for the newly discovered phases are both less than 10 GPa, similar to that of ZrB but much less than those of ZrB_2 and ZrB_{12} (about 30 GPa). In addition, the high *B/G* ratios indicate that the new compounds behave in a ductile manner, whereas all the known phases of Zr-B are brittle. The calculated band structures and PDOS results demonstrate that the new phases are metallic. Charge density distributions map suggests an ionic bonding feature between Zr and B atoms in the Zr_2B_3 and Zr_3B_2 phases. The COHP diagrams show that the atomic interaction in Zr_2B_3 phase is stronger than that in Zr_3B_2 phase and also herald Zr_2B_3 phase has a favourable stability performance. Inspired by an unexpected stoichiometries of sodium chlorides have been predicted and synthesized by high-pressure experiments[61], the current theoretical predictions will probably promote further experimental and theoretical investigation on the Zr-B system.

Acknowledgements

This work was supported by the Research Foundation of Education Bureau of Hebei Province (ZD20131039), the Natural Science Foundation of Hebei Province (E2014203243) and the NSFC (Grant No. 51121061), which is gratefully acknowledged.

State Key Laboratory of Metastable Materials Science and Technology, Yanshan University, Qinhuangdao 066004, P.R. China

** Corresponding Author E-mail: chzfan@ysu.edu.cn*

References

1 R. Kiessling, *J. Electrochem. Soc.*, 1951, **98**, 166-170.

2 G. F. Hardy and J. K. Hulm, *Phys. Rev.*, 1954, **93**, 1004-1016.

3 Q. Gu, G. Krauss and W. Steurer, *Adv. Mater.*, 2008, **20**, 3620-3626.

4 V. I. Matkovich, J. Economy, R. F. Giese Jnr and R. Barrett, *Acta Cryst.*, 1965, **19**, 1056-1058.

5 D. L. McClane, W. G. Fahrenholtz and G. E. Hilmas, *J. Am. Ceram. Soc.*, 2014, **97**, 1552-1558.

6 J. T. Norton, H. Blumenthal and S. J. Sindeband, *Trans. Am. Inst. Met.*, 1949, **185**, 749-751.

7 P. Rogl and P. E. Potter, *Calphad*, 1988, **12**, 191-204.

8 Y. Champion and S. Hagege, *Acta mater.*, 1996, **44**, 4169-4179.

9 Y. Champion and S. Hagege, *J. Mater. Sci.*, 1998, **33**, 4035-4041.

10 H. M. Chen, F. Zheng, H. S. Liu, L. B. Liu and Z. P. Jin, *J. Alloy*

Compd., 2009, **468**, 209-216.

11 A. G. Van Der Geest and A. N. Kolmogorov, *Calphad*, 2014, **46**, 184-204.

12 K. I. Romashov and V. M. Burobina, L. N. *Powder Metall. Metal Ceram*., 1970, **9**, 577-580.

13 H. Okamoto, *J. Phase Equilib*., 1993, **14**, 261-262.

14 B. Post and F. W. Glaser, *J. Chem. Phys*., 1952, **20**, 1050-1051.

15 F. W. Glaser and B. Post, *Trans. AIME*, 1953, **197**, 1117-1118.

16 E. Rudy and S. Windisch, Techn. Rept. AFML-TR-65-2. Wright Patterson AFB, Ohio. 1966, **VIII**, 1-33.

17 K. P. Portnoi, V. M. Romashov and L. I. Vyroshina, *Poroshkov. Metall*., 1970, **91**, 68-71.

18 K. I. Portnol and V. M. Romasov, Sov. *Powder Metall. Met. Ceram*., 1972, **11**, 378-384.

19 H. Nowotny, E. Rudy and F. Benesovsky, *Montash. Chem*., 1960, **91**, 963-974.

20 Y. Champion and S. Hagege, *J. Mater. Sci. Lett*., 1992, **11**, 290-293.

21 L. Bsenko, T. Lundström, *J. Less Common Met*., 1974, **34**, 273-278.

22 W. G. Fahrenholtz and G. E. Hilmas, *J. Am. Ceram. Soc*., 2007, **90**, 1347-1364.

23 M. M. Opeka, I. G. Talmy and J. A. Zaykoski, *J. Mater. Sci*., 2004, **39**, 5887-5904.

24 F. Monteverde and R. Savino, *J. Eur. Ceram. Soc.*, 2007, **27**, 4797-4805.

25 H. Wang and C.A. Wang, *J. Am. Ceram. Soc.*, 2007, **90**, 1992-1997.

26 V. Zamora, A. L. Ortiz, F. Guiberteau and M. Nygren, *J. Eur. Ceram. Soc*., 2012, **32**, 2529-2536.

27 R. Kiessling, *Acta Chem. Scand*., 1949, **3**, 90-91.

28 H. Ihara, *Phys. Rev. B*, 1977, **16**, 726-730.

29 C. N. Sun, M. C. Gupta, *J. Am. Ceram. Soc*., 2008, **91**, 1729-1731.

30 H. Li, L. Zhang, Q. Zeng, J. Wang, L. Cheng, H. Ren, Ren, K. Ren, *Comp. Mater. Sci*., 2010, **49**, 814-819.

31 B. Jäger, S. Paluch, O. J. Zogal, W. Wolf, P. Herzig and V. B. Filippov, *J. Phys.: Condens. Matter*, 2006, **18**, 2525-2535.

32 R. Fitzgerald, K. Keil and K. F. J. Heinrich, *Science*, 1968, **159**, 528-530.

33 Y. Wang, R. Lortz, Y. Paderno, V. Filippov, S. Abe, U. Tutsch and A. Junod, *Phys. Rev. B*, 2005, **72**, 024548.

34 A. V. Rybina, K. S. Nemkovski, P. A. Alekseev, J. –M. Mignot, E. S. Clementyev, M. Johnson, L. Capogna, A. V. Dukhnenko, A. B. Lyashenko and V. B. Filippov, *Phys. Rev. B*, 2010, **82**, 024302.

35 S. Thakur, D. Biswas, N. Sahadev, P. K. Biswas, G. Balakrishnan and K. Maiti, *Sci. Rep*., 2013, **3**, 3342.

36 N. Korozlu, K. Colakoglu, E. Deligoz and S. Aydin, *J. Alloy Compd*.,

2013, **546**, 157-164.

37 B. Callmer, L. Tergenius and J. O. Thomas, *J. Solid State Chem.*, 1978, **26**, 275-279.

38 A. R. Oganov and C. W. Glass. *J. Chem. Phys.*, 2006, **124**, 244704-244715.

39 A. R. Oganov, A. O. Lyakhov and M. Valle, *Acc. Chem. Res.* 2011, **44**, 227-237.

40 A. O. Lyakhov, A. R. Oganov, H. T. Stokes and Q. Zhu, *Comp. Phys. Comm*., 2013, **184***,* 1172-1182.

41 G. Kresse and J. Furthmüller, *Comput. Mater. Sci*. 1996, **6**, 15-50.

42 P. E. Blöchl, *Phys. Rev. B*, 1994, **50**, 17953-17979.

43 G. Kresse and J. Furthmüller, *Phys. Rev. B*, 1996, **54**, 11169-11186.

44 J. P. Perdew, K. Burke and M. Ernzerhof, *Phys. Rev. Lett*., 1996, **77**, 3865-3868.

45 G. Kresse and D. Joubert, *Phys. Rev. B*, 1999, **59**, 1758-1775.

46 H. J. Monkhorst and J. D. Pack, *Phys. Rev. B*, 1976, **13**, 5188-5192.

47 A. Togo, F. Oba and I. Tanaka, *Phys. Rev. B*, 2008, **78**, 134106.

48 M. D. Segall, P. J. D. Lindan, M. J. Probert, C. J. Pickard, P. J. Hasnip, S. J. Clark and M. C. Payne, *J. Phys.: Condens. Matter*, 2002, **14**, 2717-2744.

49 V. L. Deringer, A. L. Tchougréeff and R. Dronskowski, *J. Phys. Chem. A*, 2011, **115**, 5461-5466.

50 S. Maintz, V. L. Deringer, A. L. Tchougréeff and R. Dronskowski, *J. Comput. Chem.*, 2013, **34**, 2557-2567.

51 Z. J. Wu, E. J. Zhao, H. P. Xiang, X. F. Hao, X. J. Liu and J. Meng, *Phys. Rev. B*, 2007, **76**, 054115.

52 R. Hill, *Proc. Phys. Soc. A*, 1952, **65**, 349-354.

53 X. H. Zhang, X. G. Luo, J. C. Han, J. P. Li and W. B. Han, *Comput. Mater. Sci.*, 2008, **44**, 411-421.

54 S. F. Pugh, *Philos. Mag.*, 1954, **7**, 823-843.

55 X. Q. Chen, H. Niu, D. Li and Y. Li, *Intermetallic*, 2011, **19**, 1275-1281.

56 http://han.ess.sunysb.edu/hardness/

57 T. Hughbanks and R. Hoffmann, *J. Am. Chem. Soc.*, 1983, **105**, 3528-3537.

58 R. Hoffmann, *Solids and surfaces. A chemist's View of Bonding in Extended structures*, VCH, New York, 1988.

59 R. Dronskowski, *Computational Chemistry of Solid State Material*, Wiley-VCH: Weinheim, New York, 2005.

60 R. Dronskowski and P. E. Blöchl, *J. Phys. Chem.*, 1993, **97**, 8617-8624.

61 W. W. Zhang, A. R. Oganov, A. F. Goncharov, Q. Zhu, S. E. Boulfelfel, A. O. Lyakhov, M. Somayazulu and V. B. Prakapenka, *Science,*2013, **342**,1502-1505.

Table 1 Optimized Crystallographic Data of Zr_2B_3

Space group	*a* (Å)	*b* (Å)	*c* (Å)	*V* (Å^3)	*Z*
Pmmn (No. 59)	5.18	3.15	7.23	118.18	2

atom	position	*x*	*y*	*z*
Zr1	2*a*	0.0000	0.0000	0.6085
Zr2	2*b*	0.0000	0.5000	0.0124
B1	4*f*	0.8324	0.0000	0.2591
B2	2*b*	0.5000	0.0000	0.6595

Table 2 Optimized Crystallographic Data of Zr_3B_2

Space group	*a* (Å)	*b* (Å)	*c* (Å)	*V* (Å^3)	*Z*
Cmmm (No. 65)	14.49	3.16	3.45	157.87	3

atom	position	*x*	*y*	*z*
Zr1	2*a*	0.5000	0.5000	0.0000
Zr2	4*h*	0.1563	0.5000	0.5000
B1	4*g*	0.2211	0.0000	0.0000

Table 3 The Calculated values of elastic constants C_{ij} (GPa) of the newly discovered phases.

Compound	C_{11}	C_{22}	C_{33}	C_{44}	C_{55}	C_{66}	C_{12}	C_{13}	C_{23}
Zr_2B_3	373.9	388.6	359.2	122.5	52.9	19.0	94.5	82.5	107.8
Zr_3B_2	110.3	327.1	247.8	121.1	38.4	32.6	77.4	95.5	53.6

Table 4 Bulk modulus B (GPa), Shear modulus G (GPa), Young′s modulus E (GPa), Poisson′s ratio σ, and B/G ratio for the new and known phases of Zr-B, and the Vicker′s hardness H_v (GPa) for Zr_2B_3 and Zr_3B_2 from the empirical scheme (H_v^*) and Lyakhov-Oganov method ($H_v^\#$).

Compound	B	G	E	B/G	σ	H_v^*	$H_v^\#$
Zr_2B_3	115.7	57.3	147.5	2.02	0.29	6.4	7.9
Zr_3B_2	187.7	73.9	196.0	2.54	0.33	5.3	7.5
ZrB	160.6[a]	102.7[a]	253.9[a]	1.56[a]	0.24[a]	14.8	13
ZrB_2	229.1[a]	210.5[a]	483.5[a]	1.09[a]	0.15[a]	38.4	30.0
	239.0[b]	229.0[b]	520.0[b]	1.04[b]	0.14[b]	42.7	-
ZrB_{12}	243.5[c]	204.4[c]	479.1[c]	1.19[c]	0.17[c]	33.6	29.3

[a] Ref. 30 [b] Ref. 53 [c] Ref. 36

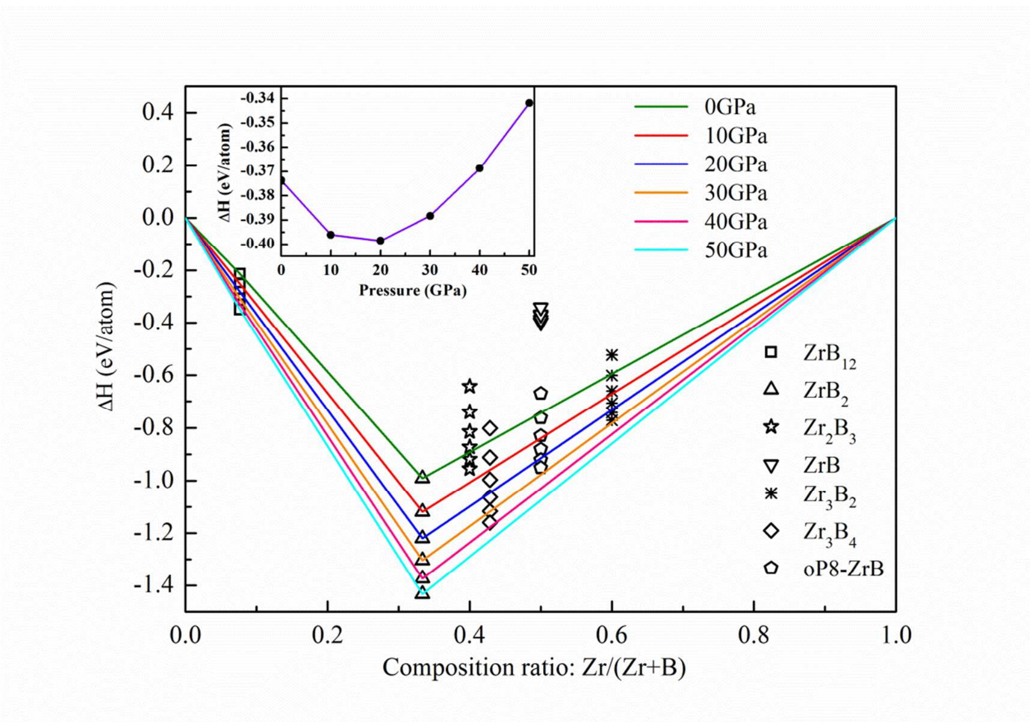

The convex hull of Zr-B system at the pressure of 0 ~ 50 GPa.

TOC